Letter

# Uniaxial versus biaxial pathways in one-dimensional cholesteric liquid crystals

Yucen Han, James Dalby, and Apala Majumdar*
*Department of Mathematics and Statistics, University of Strathclyde, Glasgow G1 1XH, United Kingdom*

Benjamin M. G. D. Carter
*H.H. Wills Physics Laboratory and Bristol Centre for Functional Nanomaterials, University of Bristol, Tyndall Avenue, Bristol BS8 1TL, United Kingdom*

Thomas Machon†
*H.H. Wills Physics Laboratory, University of Bristol, Tyndall Avenue, Bristol BS8 1TL, United Kingdom*

(Received 3 December 2021; revised 3 June 2022; accepted 27 June 2022; published 2 August 2022)

Cholesteric liquid crystals exhibit great morphological richness of static metastable states. Understanding the transitions between such states is key for the development of switchable devices. We show, using a quasi-one-dimensional model, that cholesterics exhibit distinct uniaxial and biaxial pathways between distinct minima. We study transitions between different layer numbers and prove, and show, that transition states are distinguished either through splay-mediated untwisting, understood through contact topology, or the presence of biaxiality. Furthermore we characterize a menagerie of additional saddle points that dictate the connectivity of the solution landscape.

DOI: 10.1103/PhysRevResearch.4.L032018

Cholesteric liquid crystals display rich morphology, particularly in confinement. For a given geometry, with specified boundary conditions, one typically finds a huge variety of metastable states [1]. These include arbitrarily knotted disclination lines [2–5], torons [6,7] and Hopf solitons [8], inverse torons [9], point defect constellations [10,11], complex patterns in shells, cylinders and droplets [12–16], and Skyrmion lattices [17] amongst many others. This richness gives cholesteric liquid crystals great potential for the creation of soft devices. There is another key strength to cholesterics and all liquid crystal systems, they flow (spontaneously in the case of active systems) and readily respond to applied fields [18]; in other words, they are switchable. For a switchable device, understanding and controlling pathways between stable states is just as important as understanding the stable states themselves, non-energy-minimizing critical points play crucial roles in switching mechanics and selection of minimizers [19]. In a cholesteric system, chirality leads to many complex metastable configurations and one expects similar richness in the space of transition pathways between metastable states.

Many liquid crystalline configurations are distinguished by their topology, using homotopy theoretic invariants [20–22]. However, these invariants often cannot distinguish between two cholesteric configurations that appear qualitatively distinct. We consider the simplest example in this letter [23]; the number of layers in a cholesteric cell, with all even (or odd) layer numbers equivalent from a homotopy-theoretic perspective. An alternative approach uses ideas from contact topology [9,11,23] to provide more sophisticated topological invariants. In this theory, the key role is played by the twist density; if the twist density is nowhere-zero, the liquid crystal configuration is labeled as being chiral. Using the tools of contact topology [24], one can rigorously define new invariants (e.g., the layer number [9,23,25]) that can distinguish between chiral configurations, for example helices with different numbers of twists/layers. This gives a new heuristic understanding of the cholesteric solution landscape, which we explore in this letter. We investigate pathways between helices with different numbers of twists, and use sophisticated topological and numerical studies to discover a dichotomy; the helices or equivalently the different chiral sectors can be connected by"untwisted states" or they can be connected by exotic biaxial defects, which avoid the untwisting. Which pathway is preferred or observed is a delicate question that depends on the geometry, temperature, and material properties, and careful investigations of the parameter space can allow us to steer these pathways and manipulate the corresponding solution landscapes. Our work is a first step in the theoretical demonstration of such dichotomies for the simplest model cholesteric system, and our tools will extend to more complex higher-dimensional cholesteric systems to navigate through the labyrinth of metastable states and the pathways between them.

We study a cholesteric sample inside a cell of height $h$, $\Omega = \{(x, y, z) \in \mathbb{R}^3 | \ 0 \leqslant z \leqslant h\}$. We work in the powerful

*apala.majumdar@strath.ac.uk
†t.machon@bristol.ac.uk

Landau–de Gennes (LdG) formalism, where the cholesteric state is described by the LdG $\mathbf{Q}$-tensor order parameter, with Cartesian components $Q_{ij}$. The LdG $\mathbf{Q}$-order parameter is a symmetric, traceless $3 \times 3$ matrix [26]

$$\mathbf{Q} = \sum_{i=1}^{3} \lambda_i \mathbf{e}_i \otimes \mathbf{e}_i,$$

where the eigenvectors, $\mathbf{e}_i$, model the preferred material directions and the corresponding eigenvalues, $\lambda_i$, measure the degree of orientational order about $\mathbf{e}_i$. The eigenvector with the largest positive eigenvalue is the nematic director $\mathbf{n}$ [26]. A $\mathbf{Q}$-tensor is uniaxial if it has two equal nonzero eigenvalues and biaxial if it has three distinct eigenvalues [27]. In particular, $\mathbf{Q}$ is said to be quasi-uniaxial if it has nonzero eigenvalues and a well-defined director, and maximally biaxial if it has a single zero eigenvalue.

Assuming translational symmetry in the $x$ and $y$ directions, the equilibrium or physically observable cholesteric states correspond to minimizers of the non-dimensionalized cholesteric energy per unit area [28]

$$\begin{aligned}\bar{F}(\mathbf{Q}) &= \frac{hF(\mathbf{Q})}{K_0} \\ &= \int_0^1 \left\{ \frac{1}{4}(\overline{\nabla} \cdot \mathbf{Q})^2 + \frac{\eta}{4}|\overline{\nabla} \times \mathbf{Q} + 2\sigma \mathbf{Q}|^2 + \lambda \frac{f_b(\mathbf{Q})}{C} \right\} d\bar{z}. \end{aligned} \tag{1}$$

The elastic energy density has splay/bend [29] and twist contributions: $\eta = K_1/K_0$ is the ratio of the twist and splay/bend elastic constants and quantifies the elastic anisotropy; $\sigma/2\pi = h/p_0$ where $p_0$ is the pitch of the cholesteric, gives the number of $2\pi$ rotations of the director in the $z$ direction; and $\lambda = \frac{h^2 C}{K_0}$ is a measure of domain height/size with $C$ a material-dependent positive constant. Using the parameter values in Refs. [30,31], a typical value is $\eta = \frac{1}{2}$. The values of $\eta$ can be tailored by the material such as 5CB and PBG [32]. We omit bars from rescaled variables. The bulk energy density is

$$f_b(\mathbf{Q}) := \frac{A}{2}\mathrm{tr}\mathbf{Q}^2 - \frac{B}{3}\mathrm{tr}\mathbf{Q}^3 + \frac{C}{4}(\mathrm{tr}\mathbf{Q}^2)^2, \tag{2}$$

and dictates the isotropic-nematic phase transition as a function of temperature. The variable $A = \alpha(T - T^*)$ is a rescaled temperature, with $T^*$ a characteristic temperature, and $B > 0$ is material dependent constant ($C$ is as above) [26]. Typical values for the liquid crystal MBBA are, $\alpha = -0.042 \times 10^6$ N/(K m$^2$), $B = 0.64 \times 10^6$ N/m$^2$, and $C = 0.35 \times 10^6$ N/m$^2$, as used in our numerical simulations. We work with low temperatures for which $A < 0$, so the set of $f_b$ minimizers are uniaxial $\mathbf{Q}$-tensors, of the form $\mathbf{Q} = s_+(\mathbf{n} \otimes \mathbf{n} - \mathbf{I}/3)$, for arbitrary unit-vectors fields or nematic directors, $\mathbf{n}$. Here $s_+ = (B + \sqrt{B^2 + 24|A|C})/4C$.

We impose Dirichlet boundary conditions on the top and bottom of the cell, given by $\mathbf{Q}(z = 0) = \mathbf{Q}(z = h) = s_+(\mathbf{e}_x \otimes \mathbf{e}_x - \mathbf{I}/3)$, where $\mathbf{e}_x$ is a unit vector in the $x$ direction. This is equivalent to including a Rapini-Papoular surface energy in the limit of infinite surface anchoring. In the weak anchoring regime, the pathway may proceed via transitions at the boundary [33–35]. We focus on helical director fields

$$\mathbf{n}_w = (\cos(\pi w z/h), \sin(\pi w z/h), 0),$$

with $w \in \mathbb{Z}$ the twisting or layer number, and define the associated uniaxial $\mathbf{Q}$-tensor to be $\mathbf{Q}_w = s_+(\mathbf{n}_w \otimes \mathbf{n}_w - \frac{\mathbf{I}}{3})$. Deep in the cholesteric phase, the cholesteric free energy will be minimized by a quasi-uniaxial $\mathbf{Q}$-tensor close to $\mathbf{Q}_w$ (with a small degree of biaxiality [36]). Such a helical texture will satisfy the boundary conditions only if the pitch $p$ satisfies $p = h/|w|$. Otherwise the system encounters geometric frustration and one typically finds a number of metastable helices, with different twisting numbers $w$ [37].

We are interested in pathways between different $\mathbf{Q}_w$, exploiting the full freedom of the $\mathbf{Q}$-tensor formalism. There is a qualitative difference between an $w - 1 \to w$ transition and a $w - 1 \to w + 1$ transition. In the first case, the parity changes so that a pathway with fixed boundary conditions, will exhibit a defect in $\mathbf{n}$, or a point of maximal biaxiality in $\mathbf{Q}$. On the other hand, weak anchoring could allow for a defect-free pathway by deforming the texture at the boundary, as has recently been studied in the interesting Refs. [33,34,38]. In this case, the authors observe an interesting dichotomy between in-plane director slippage and an out-of-plane pathway, which has a visual resemblance to the uniaxial pathway observed here (Fig. 1, uniaxial state $S2$), whether this connection has deeper significance remains to be seen. For a $w - 1 \to w + 1$ transition, there is no analogous constraint and a defect-free quasiuniaxial pathway is admissible, but there are hidden topological constraints of untwisting and splay along such quasiuniaxial pathways, as demonstrated in the two theorems below.

*Theorem 1.* The director field $\mathbf{n}$ along any quasi uniaxial pathway between $\mathbf{Q}_{w_1}$ and $\mathbf{Q}_{w_2}$, for $w_1 \neq w_2$, must untwist, that is $\mathbf{n} \cdot \nabla \times \mathbf{n}$ must vanish at some point in space and time along the pathway.

This is a refinement of a result given in Refs. [23], and is related to a number of results in contact topology [24,39,40]. A proof is given in the Supplemental Material (SM) [41]. Topologically required untwisting can also be observed near point defects in cholesterics [11,42]. Since cholesterics prefer to twist, with the term $(\mathbf{n} \cdot \nabla \times \mathbf{n} + \sigma)^2$ in the Frank free energy, the topologically required untwisting predicts a chiral energy barrier between different values of $w$.

Next, consider a pathway with zero splay ($\nabla \cdot \mathbf{Q} = 0$), such as a linear interpolation between $\mathbf{Q}_{\omega-1}$ and $\mathbf{Q}_{\omega+1}$. If we restrict ourselves to $\mathbf{Q}$-tensors with zero splay, then we necessarily have

$$Q'_{13} = Q'_{23} = Q'_{33} = 0. \tag{3}$$

Denoting the pathway by $\mathbf{Q}(t, z)$, we have $\mathbf{Q}(t = 0) = \mathbf{Q}_{\omega-1}$ and $\mathbf{Q}(t = 1) = \mathbf{Q}_{\omega+1}$, with $Q_{13} = Q_{23} = 0$ and $Q_{33} = -s_+/3 < 0$ for all $t \in [0, 1]$, so that the nematic director is always in the $xy$ plane and is splay free. The leading-order energy is

$$\begin{aligned} F(\mathbf{Q}) &= F(\mathbf{q}) \\ &= \int_0^1 \left\{ \frac{\eta}{2}|\nabla \mathbf{q}|^2 + 2\sigma\eta(\mathbf{q} \cdot \nabla \times \mathbf{q}) \right. \\ &\quad \left. + \frac{\lambda}{C}\tilde{f}_b(s_+, |\mathbf{q}|^2) + C_0(s_+, \eta, \sigma) \right\} dz, \end{aligned} \tag{4}$$

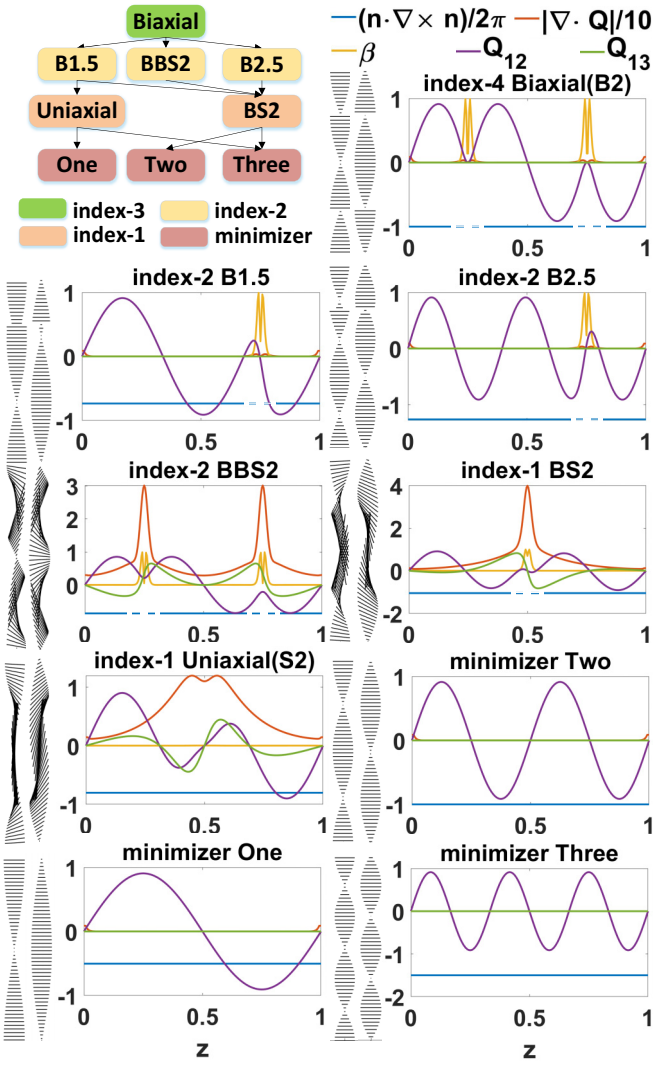


FIG. 1. The solution landscape with $\lambda = 3500$, $\eta = 4.5$, $\sigma = 2\pi$, $A = -B^2/3C$. We plot the twisting measure $(n \cdot \nabla \times n)/2\pi$ (represented by dashed line near biaxial torus), the splay/bend measure $|\nabla \cdot \mathbf{Q}|/10$, the biaxiality measure $\beta = 1 - 6\frac{(tr\mathbf{Q}^3)^2}{|\mathbf{Q}|^6}$, the twisting in $xy$ plane $Q_{12}$ and the out-of-plane order $Q_{13}$. We label the critical points as follows: B indicates the presence of biaxial tori, S indicates the presence of large splay, and the number at the end is the amount of rotation in the $xy$ plane, in units of $\pi$. The index-4 *Biaxial*$(B2)$ state has two biaxial tori and has unstable directions that tune the twisting periods and connect with the stable *One* and *Three* states. The *Biaxial* state connects with three index-2 critical points, $B1.5$, $B2.5$, and $BBS2$. $B1.5$ and $B2.5$ have only one biaxial torus, with $3\pi/2$ and $5\pi/2$ twisting and connect *One* and *Two*, and *Two* and *Three*, respectively. $BBS2$ has a more complex profile with two biaxial tori, $2\pi$ twisting, and splay. The defect-free index-1 *Uniaxial*$(S2)$ state, is the transition state between the stable *One* and *Three* states. $BS2$ is the transition state between the stable $\mathbf{Q}_2$ and $\mathbf{Q}_3$.

where $\mathbf{q} = (\frac{Q_{11}-Q_{22}}{2}, Q_{12})$ and $C_0$ is a function depending on $s_+$, $\eta$, and $\sigma$, i.e., there are only two degrees of freedom in the class of splay free configurations. Equation (4) bears considerable similarity to a one-dimensional model studied by Golovaty *et al.* [43]. In the reduced description (4), the boundary conditions are $\mathbf{q} = (s_+/2, 0)$ at the top and bottom of the cell. In the helical state $\mathbf{Q}_w$, the vector $\mathbf{q}$ winds by $2w\pi$ between the top and bottom. The change in winding number across the cell height forces a zero in $\mathbf{q}$, and points of maximal biaxiality correspond to $|\mathbf{q}| = s_+/6$. Thus, any splay-free pathway must cross the circle of maximal biaxiality as stated below:

*Theorem 2.* Any smooth zero-splay and bend pathway ($\nabla \cdot \mathbf{Q} = 0$) between $\mathbf{Q}_{w_1}$ and $\mathbf{Q}_{w_2}$, $w_1 \neq w_2$, must contain points of maximal biaxiality.

A full proof, and slight generalization, is given in the SM. Theorem 1 implies that the director field along any quasi-uniaxial pathway must untwist. Theorem 2 implies any quasiuniaxial pathway must also have nonzero splay/bend. This reflects the large number of complex compatibility conditions [44–46] that relate the different deformation modes (splay, twist, bend, biaxial splay [46–48]) of a director field. We note this as the twist elastic constant can be substantially smaller than the splay or bend constants [32]. Combined, these two Theorems show that any pathway that changes the twisting number can either introduce defects (maximal biaxiality) or untwist (or both), and this conclusion applies to any pathway, not just pathways between minimizers of the free energy but also to pathways between distinct non-equilibrium states in hydrodynamic flows, where energy principles may not exist [49–51].

In Fig. 1, we illustrate this dichotomy in pathways between $\mathbf{Q}_\omega$, by looking at the critical points of the energy (1) for a large cell with $\lambda = 3500$ and $\eta = 4.5$. In the $\lambda \to \infty$ limit, the bulk energy dominates and energy minimizers tend to be approximately uniaxial, i.e., solutions of the Euler-Lagrange equations in the restricted space of bulk energy minimizers [52]. The leading order minimizer profiles are the helical states $\mathbf{Q}_\omega$, with $\omega = \frac{\sigma}{\pi}$. We fix $\sigma = 2\pi$ in what follows and focus on (transition) pathways between three locally stable critical points of the free energy in Fig. 1: $\mathbf{Q}_1$ (*One*, $\pi$ twisting), $\mathbf{Q}_2$ (*Two*, $2\pi$ twisting) and $\mathbf{Q}_3$ (*Three*, $3\pi$ twisting). The *One* and *Three*-helical states have the same energy for any $\lambda$, $\eta$, and $K_0$, whilst $\mathbf{Q}_2$ has the minimum energy amongst the three helical states.

To compute these pathways, we numerically compute solutions of the Euler-Lagrange equations for (1), which are critical points of the free energy. The Morse index of a critical point is the number of negative eigenvalues of the corresponding Hessian of the free energy, evaluated at the critical point [53]. Minimizers (local and global) have index-0, index-$k$ saddle points are unstable in $k$ distinguished eigendirections. We use the high-index optimization-based shrinking dimer (HiOSD) method [54] and upward/downward search algorithms [55], to compute sample solution landscapes in Fig. 1 (see SM).

To find novel biaxial critical points, we construct an initial condition with $2\pi$ twisting in the $xy$ plane, but with two discontinuous points of the nematic director, where $\mathbf{q} = 0$ (see SM). Using Newton's method and this initial condition, we can obtain a splay-free critical point, labeled as the *Biaxial* solution (see Fig. 1), for various $\lambda$ and $\eta$. The *Biaxial* solution has two biaxial tori around the discontinuous points, and each biaxial torus contains two points of maximal biaxiality and a point of uniaxiality at the center. The biaxial torus is a

universal defect structure arising from topological constraints [56], and can be understood in part by the proof of Theorem 2 in the SM. For sufficiently small $K_0$ (when splay is not heavily penalized), the *Biaxial* solution is an unstable saddle point (index >1), and the Morse index of the *Biaxial* state increases as $\lambda$ increases.

With the *Biaxial* state as the parent state (state with highest index), we compute the solution landscape for $\lambda = 3500$ (corresponding to a small cell of about $0.2\mu m$ height), and $\eta = 4.5$, in Fig. 1. The computation reveals a menagerie of critical points, which we classify broadly as either quasiuniaxial or biaxial (without and with maximal biaxiality) and with and without splay (nonzero and zero $|\nabla \cdot \mathbf{Q}|$, respectively). We observe, in passing, that the index of the biaxial critical points is twice the number of biaxial tori in the splay-free case, and equal to the number of biaxial tori with splay in Fig. 1. Notably, we find two competing pathways between the stable uniaxial *One* and *Three*-helical states. According to Fig. 1, there is the uniaxial pathway via the index-1 *Uniaxial* state, and the biaxial pathway via the index-4 *Biaxial* state. Theorem 1 implies that the uniaxial pathway must untwist (i.e., have $\mathbf{n} \cdot \nabla \times \mathbf{n} = 0$ at some point) and, as suggested by Theorem 2, this untwisting is mediated by splay. On the other hand, the *Biaxial* state, *B*2, is splay-free and indeed the entire pathway in this case can be chosen in the class of splay-free configurations (4).

Recent work has found similar structures to (half of) our uniaxial pathway in boundary-driven unwinding transitions, this suggests that the uniaxial critical point may become further preferred under an applied electric field, beyond the Fréedericksz transition [33,34]. Such out-of-plane pathways may be also be relevant in the study of helical axis transitions [57]. A related set of uniaxial untwisting pathways in nematics were considered by Goldbart and Ao [58,59].

The question then is, which pathway is preferred? This then depends on $\eta$, $\lambda$, and the temperature. In the $K_0 \to \infty$ limit, (1), only the splay-free states: *Biaxial*(*B*2), *B*1.5, *B*2.5, *One*, *Two*, and *Three*, survive as critical points. In particular, the *Biaxial* state is always a critical point of Eq. (1) for all $K_0$, and the index of *Biaxial* state decreases from 4, to 3, to 2, to 0, as $K_0$ increases from 1 to $\infty$. The *Uniaxial*(*S*2), *BS*2, and *BBS*2, have splay; their Morse indices and energy increase with $K_0$. As temperature decreases, uniaxiality is energetically preferred to biaxiality. The *Biaxial*(*B*2), *B*1.5, *B*2.5, *BS*2, and *BBS*2 critical points have points of maximal biaxiality, they have increasing energy and Morse indices with decreasing temperature, in contrast to the *Uniaxial*(*S*2), *One*, *Two*, and *Three* which have decreasing energy with decreasing temperature.

Returning now to the choice between the biaxial (*B*2) and uniaxial (*S*2) pathways, the energy barrier of the pathway is the energy difference between either the *Uniaxial*(*S*2) or *Biaxial*(*B*2) critical point, and the stable *One* (or *Three*) states. The difference between two energy barriers is equal to the energy difference between *Uniaxial*(*S*2) and *Biaxial*(*B*2). When the temperature is high, the energy difference is low since uniaxiality is only weakly preferred. The uniaxial pathway cannot be observed for extreme parameter values, such as large $K_0$. More importantly, for the range of $A$ and $\eta$ considered in Figure 2, for small and large $\lambda$, the uniaxial pathway is always energetically preferable but the uniaxial and biaxial pathways have comparable energy barriers, so that experimental observations of both pathways are possible in practice.

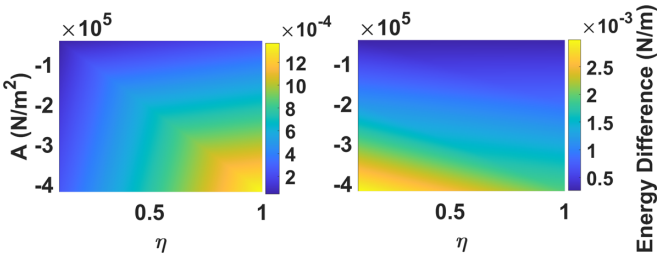


FIG. 2. The difference between energy barriers [the energy $F$ before nondimensionalization in Eq. (1)] of the uniaxial and biaxial pathways as a function of the re-scaled temperature, $A$ and elastic anisotropy $\eta$. Left: small cell with $\lambda = 3500$ ($h \approx 0.2\,\mu$m); Right: large cell with $\lambda = 17500$ ($h \approx 1.4\,\mu$m).

What are the implications for experiments? During coarsening or other dynamic processes (for example, the Helfrich-Hurault instability [60]) cholesterics will typically undergo morphological changes whereby layer numbers are observed to change in a discrete fashion. Our work suggests that a cholesteric system can choose to mediate such a transition by either untwisting via splay and bend distortions, or through biaxiality (defects). Experimentally verifiable optical signatures for these states as well as their pathways are shown in the SM. Our findings illustrate that biaxiality may become experimentally observable for these toy systems, with high temperature and large $K_0$, either as equilibria or in pathways between distinct equilibria. Further, we conjecture that we can construct hierarchies of LdG critical points from building points, e.g., the biaxial torus or untwisting states (the work of Goldbart and Ao suggests that the barriers we study increase with the number of twists [58,59]). In higher dimensions, cholesterics exhibit great morphological richness, knotted disclination lines [2–5] and Hopf solitons [8], for example. Whether the ideas discussed in this letter can be used to study transition pathways for these complex problems, remains an interesting open question (we note biaxial tori are expected to be minimizing for certain problems [56]), and our major challenge is to discover universal principles for solution landscapes of confined soft matter systems.

T.M. and B.M.G.D.C. proposed the problem, T.M. conceived and proved Theorems 1 and 2. A.M. led the asymptotic analysis and mathematical modelling part of the manuscript. Y.H. performed the numerical simulations; Y.H. and J.D. carried out the analysis; B.M.G.D.C. performed initial numerical simulations. Y.H., J.D., B.M.G.D.C., A.M. and T.M. contributed to the manuscript writing and revision.

A.M. J.D., and Y.H. gratefully acknowledge support from a Heilbronn Small Grant that facilitated this collaboration. Y.H. is supported by a Royal Society Newton International Fellowship. The authors thank Y. Wang for sharing computational code for optical profiles. T.M. and B.M.G.D.C. acknowledge funding from EPSRC with Grant code EP/L016648/1.

[1] I. M. Tambovtsev, A. O. Leonov, I. S. Lobanov, A. D. Kiselev, and V. M. Uzdin, Topological structures in chiral media: Effects of confined geometry, Phys. Rev. E **105**, 034701 (2022).

[2] U. Tkalec, M. Ravnik, S. Čopar, S. Žumer, and I. Muševič, Reconfigurable knots and links in chiral nematic colloids, Science **333**, 62 (2011).

[3] J.-S. B. Tai and I. I. Smalyukh, Three-dimensional crystals of adaptive knots, Science **365**, 1449 (2019).

[4] T. Machon and G. P. Alexander, Knotted Defects in Nematic Liquid Crystals, Phys. Rev. Lett. **113**, 027801 (2014).

[5] T. Machon and G. P. Alexander, Knots and nonorientable surfaces in chiral nematics, Proc. Natl. Acad. Sci. USA **110**, 14174 (2013).

[6] I. I. Smalyukh, Y. Lansac, N. A. Clark, and R. P. Trivedi, Three-dimensional structure and multistable optical switching of triple-twisted particle-like excitations in anisotropic fluids, Nat. Mater. **9**, 139 (2010).

[7] B. G.-ge Chen, P. J. Ackerman, G. P. Alexander, R. D. Kamien, and I. I. Smalyukh, Generating the Hopf Fibration Experimentally in Nematic Liquid Crystals, Phys. Rev. Lett. **110**, 237801 (2013).

[8] P. J. Ackerman and I. I. Smalyukh, Diversity of Knot Solitons in Liquid Crystals Manifested by Linking of Preimages in Torons and Hopfions, Phys. Rev. X **7**, 011006 (2017).

[9] J. Eun, J. Pollard, S.-J. Kim, T. Machon, and J. Jeong, Layering transitions and metastable structures of cholesteric liquid crystals in cylindrical confinement, Proc. Natl. Acad. Sci. USA **118**, e2102926118 (2021).

[10] G. Posnjak, S. Čopar, and I. Muševič, Hidden topological constellations and polyvalent charges in chiral nematic droplets, Nat. Commun. **8**, 14594 (2017).

[11] J. Pollard, G. Posnjak, S. Čopar, I. Muševič, and G. P. Alexander, Point Defects, Topological Chirality, and Singularity Theory in Cholesteric Liquid-Crystal Droplets, Phys. Rev. X **9**, 021004 (2019).

[12] A. Darmon, M. Benzaquen, S. Čopar, O. Dauchot, and T. Lopez-Leon, Topological defects in cholesteric liquid crystal shells, Soft Matter **12**, 9280 (2016).

[13] Y. Bouligand and F. Livolant, The organization of cholesteric spherulites, J. Phys. France **45**, 1899 (1984).

[14] A. Darmon, M. Benzaquen, D. Seč, S. Čopar, O. Dauchot, and T. Lopez-Leon, Waltzing route toward double-helix formation in cholesteric shells, Proc. Natl. Acad. Sci. USA **113**, 9469 (2016).

[15] L. Tran, M. O. Lavrentovich, G. Durey, A. Darmon, M. F. Haase, N. Li, D. Lee, K. J. Stebe, R. D. Kamien, and T. Lopez-Leon, Change in Stripes for Cholesteric Shells via Anchoring in Moderation, Phys. Rev. X **7**, 041029 (2017).

[16] D. B. Emerson, P. E. Farrell, J. H. Adler, S. P. MacLachlan, and T. J. Atherton, Computing equilibrium states of cholesteric liquid crystals in elliptical channels with deflation algorithms, Liq. Cryst. **45**, 341 (2018).

[17] J.-i. Fukuda and S. Žumer, Quasi-two-dimensional skyrmion lattices in a chiral nematic liquid crystal, Nat. Commun. **2**, 246 (2011).

[18] E. C. Gartland Jr., H. Huang, O. Lavrentovich, P. Palffy-Muhoray, I. Smalyukh, T. Kosa, and B. Taheri, Electric-field induced transitions in a cholesteric liquid-crystal film with negative dielectric anisotropy, J. Comput. Theor. Nanosci. **7**, 709 (2010).

[19] Y. Han, J. Yin, P. Zhang, A. Majumdar, and L. Zhang, Solution landscape of a reduced Landau–de Gennes model on a hexagon, Nonlinearity **34**, 2048 (2021).

[20] N. D. Mermin, The topological theory of defects in ordered media, Rev. Mod. Phys. **51**, 591 (1979).

[21] G. P. Alexander, B. G.-ge Chen, E. A. Matsumoto, and R. D. Kamien, Colloquium: Disclination loops, point defects, and all that in nematic liquid crystals, Rev. Mod. Phys. **84**, 497 (2012).

[22] V. Poenaru and G. Toulouse, The crossing of defects in ordered media and the topology of 3-manifolds, J. Phys. France **38**, 887 (1977).

[23] T. Machon, Contact topology and the structure and dynamics of cholesterics, New J. Phys. **19**, 113030 (2017).

[24] H. Geiges, *An Introduction to Contact Topology* (Cambridge University Press, Cambridge, 2008), Vol. 109.

[25] Y. Hu and T. Machon, Stability of highly-twisted skyrmions from contact topology, arXiv:2102.13126.

[26] P. G. de Gennes, *The Physics of Liquid Crystals* (Oxford University Press, Oxford, 1974).

[27] A. Majumdar, Equilibrium order parameters of nematic liquid crystals in the Landau–de Gennes theory, Euro. J. Appl. Math. **21**, 181 (2010).

[28] J. Fukuda and S. Žumer, Cholesteric blue phases: effect of strong confinement, Liq. Cryst. **37**, 875 (2010).

[29] The splay term contains bend distortions also.

[30] E. Priestly, *Introduction to Liquid Crystals* (Springer Science & Business Media, New York, 2012).

[31] N. J. Mottram and C. J. Newton, Introduction to q-tensor theory, arXiv preprint arXiv:1409.3542.

[32] C. F. Dietrich, P. J. Collings, T. Sottmann, P. Rudquist, and F. Giesselmann, Extremely small twist elastic constants in lyotropic nematic liquid crystals, Proc. Natl. Acad. Sci. USA **117**, 27238 (2020).

[33] S. S. Tenishchev, A. D. Kiselev, A. V. Ivanov, and V. M. Uzdin, Multiple minimum-energy paths and scenarios of unwinding transitions in chiral nematic liquid crystals, Phys. Rev. E **100**, 062704 (2019).

[34] S. S. Tenishchev, I. M. Tambovtcev, A. D. Kiselev, and V. M. Uzdin, Hysteresis and Fréedericksz thresholds for twisted states in chiral nematic liquid crystals: Minimum-energy path approach, J. Mol. Liq. **325**, 115242 (2021).

[35] G. Barbero, W. Zheng, and B. Zappone, Twist transitions and force generation in cholesteric liquid crystal films, J. Mol. Liq. **267**, 242 (2018).

[36] D. C. Wright and N. D. Mermin, Crystalline liquids: the blue phases, Rev. Mod. Phys. **61**, 385 (1989).

[37] A. D. Kiselev and T. J. Sluckin, Twist of cholesteric liquid crystal cells: stability of helical structures and anchoring energy effects, Phys. Rev. E **71**, 031704 (2005).

[38] A. V. Ivanov, P. F. Bessarab, E. V. Aksenova, V. P. Romanov, and V. M. Uzdin, Energy surface and minimum energy paths for Fréedericksz transitions in bistable cholesteric liquid crystals, Phys. Rev. E **93**, 042708 (2016).

[39] K. Honda, On the classification of tight contact structures I. Geom. Topol. **4**, 309 (2000).

[40] K. Yutaka, The classification of tight contact structures on the 3-torus, Commun. Anal. Geom. **5**, 413 (1997).

[41] See Supplemental Material at http://link.aps.org/supplemental/10.1103/PhysRevResearch.4.L032018 for proofs of Theorems 1 and 2, details of numerical methods and optical modelling.

[42] P. J. Ackerman and I. I. Smalyukh, Reversal of helicoidal twist handedness near point defects of confined chiral liquid crystals, Phys. Rev. E **93**, 052702 (2016).

[43] D. Golovaty, M. Novack, and P. Sternberg, A one-dimensional variational problem for cholesteric liquid crystals with disparate elastic constants, J. Diff. Equ. **286**, 785 (2021).

[44] J. Pollard and G. P. Alexander, Intrinsic geometry and director reconstruction for three-dimensional liquid crystals, New J. Phys. **23**, 063006 (2021).

[45] L. C. da Silva and E. Efrati, Moving frames and compatibility conditions for three-dimensional director fields, New J. Phys. **23**, 063016 (2021).

[46] J. V. Selinger, Director deformations, geometric frustration, and modulated phases in liquid crystals, Annu. Rev. Condens. Matter Phys. **13**, 49 (2022).

[47] J. V. Selinger, Interpretation of saddle-splay and the Oseen-Frank free energy in liquid crystals, Liq. Cryst. Rev. **6**, 129 (2018).

[48] T. Machon and G. P. Alexander, Umbilic Lines in Orientational Order, Phys. Rev. X **6**, 011033 (2016).

[49] X. Tang and J. V. Selinger, Minimization principle for shear alignment of liquid crystals, Phys. Rev. E **101**, 032701 (2020).

[50] P. Pieranski and M. H. Godinho, Tropisms of the dowser texture, Materials **13**, 4681 (2020).

[51] S. Čopar, Ž. Kos, T. Emeršič, and U. Tkalec, Microfluidic control over topological states in channel-confined nematic flows, Nat. Commun. **11**, 1 (2020).

[52] A. Majumdar and A. Zarnescu, Landau–de Gennes theory of nematic liquid crystals: the Oseen–Frank limit and beyond, Arch. Ration. Mech. Anal. **196**, 227 (2010).

[53] J. Milnor, *Morse Theory* (Princeton University Press, Princeton, NJ, 1963).

[54] J. Yin, L. Zhang, and P. Zhang, High-index optimization-based shrinking dimer method for finding high-index saddle points, SIAM J. Sci. Comput. **41**, A3576 (2019).

[55] J. Yin, Y. Wang, J. Z. Y. Chen, P. Zhang, and L. Zhang, Construction of a Pathway Map on a Complicated Energy Landscape, Phys. Rev. Lett. **124**, 090601 (2020).

[56] D. Henao, A. Majumdar, and A. Pisante, Uniaxial versus biaxial character of nematic equilibria in three dimensions, Calc. Var. Partial Differ. Equ. **56**, 55 (2017).

[57] Z.-g. Zheng, Y. Li, H. K. Bisoyi, L. Wang, T. J. Bunning, and Q. Li, Three-dimensional control of the helical axis of a chiral nematic liquid crystal by light, Nature (London) **531**, 352 (2016).

[58] P. Goldbart and P. Ao, Intrinsic Torsional Viscosity of Nematic Liquid Crystals, Phys. Rev. Lett. **64**, 910 (1990).

[59] P. Goldbart and P. Ao, Intrinsic torsional viscosity in a narrow tube of nematic liquid crystal, Mol. Cryst. Liq. Cryst. **198**, 455 (1991).

[60] C. Blanc, G. Durey, R. D. Kamien, T. Lopez-Leon, M. O. Lavrentovich, and L. Tran, Helfrich-Hurault elastic instabilities driven by geometrical frustration, arXiv:2109.14668.